Single Shot Spatial and Temporal Coherence Properties of the SLAC Linac Coherent Light Source in the Hard X-Ray Regime

C. Gutt,[1,*] P. Wochner,[2] B. Fischer,[1] H. Conrad,[1] M. Castro-Colin,[2] S. Lee,[1,3] F. Lehmkühler,[1] I. Steinke,[1] M. Sprung,[1] W. Roseker,[1] D. Zhu,[3] H. Lemke,[3] S. Bogle,[2] P. H. Fuoss,[4] G. B. Stephenson,[4] M. Cammarata,[3] D. M. Fritz,[3] A. Robert,[3] and G. Grübel[1]

[1]*Deutsches Elektronen-Synchrotron (DESY), Notkestraße 85, D-22607 Hamburg, Germany*
[2]*Max-Planck-Institut für Intelligente Systeme, Heisenberg Straße 3, D-70569 Stuttgart, Germany*
[3]*LCLS, SLAC National Accelerator Laboratory, Menlo Park, California 94025, USA*
[4]*Materials Science Division, Argonne National Laboratory, 9700 South Cass Avenue, Argonne, Illinois 60439 USA*

(Received 20 September 2011; published 11 January 2012)

We measured the transverse and longitudinal coherence properties of the Linac Coherent Light Source (LCLS) at SLAC in the hard x-ray regime at 9 keV photon energy on a single shot basis. Speckle patterns recorded in the forward direction from colloidal nanoparticles yielded the transverse coherence properties of the focused LCLS beam. Speckle patterns from a gold nanopowder recorded with atomic resolution allowed us to measure the shot-to-shot variations of the spectral properties of the x-ray beam. The focused beam is in the transverse direction fully coherent with a mode number close to 1. The average number of longitudinal modes behind the Si(111) monochromator is about 14.5 and the average coherence time $\tau_c = (2.0 \pm 1.0)$ fs. The data suggest a mean x-ray pulse duration of (29 ± 14) fs behind the monochromator for (100 ± 14) fs long electron pulses.

DOI: 10.1103/PhysRevLett.108.024801 PACS numbers: 41.60.Cr, 41.50.+h, 61.05.cf

The Linac Coherent Light Source (LCLS) was the first x-ray free-electron laser to lase in the hard x-ray regime at 1.5 Å wavelength [1]. The ultrashort pulse duration of ≤ 100 fs in combination with short wavelength light offers the prospect to image structure and dynamics on atomic spatial and temporal scales with important applications in the biological [2,3] and material sciences [4]. In materials science it is, e.g., envisioned to take single shot images of molecular liquids to unravel bond order in disordered structures [5], to follow dynamic properties via photon correlation techniques [6], or to image magnetic spins [7,8] on their intrinsic time scales. Many of the exciting proposed experimental techniques rely on the coherence properties of the hard x-ray beam since the ultrashort pulse duration promises the possibility to take single shot speckle patterns undisturbed from any thermal motion within the sample.

The coherence properties of light sources based on self-amplified spontaneous emission (SASE) differ from those of conventional optical lasers as the SASE process arises from random fluctuations in the electron beam [9]. Since shot noise in the electron beam is a stochastic process, the SASE generated x-ray radiation also possesses certain random features. Simulations predict, for example, that a single SASE free-electron laser pulse consists of several spectral spikes or longitudinal modes [10–12]. In contrast, the transverse coherence length is predicted to be better defined. Experiments at the free-electron laser FLASH operating in the vacuum ultraviolet regime confirmed those simulations [13–16]. The coherence properties of the LCLS in the soft x-ray regime has been reported recently [17].

Measuring the transverse and longitudinal coherence properties of hard x-ray beams is a nontrivial task because of the small length scales involved. We propose and demonstrate here an avenue for measuring the coherence properties in the hard x-ray regime that is based on measuring coherent diffraction speckle patterns of disordered samples. The statistical properties of such speckle patterns are directly related to the coherence properties of the incoming radiation field [18], and thus allow us to determine the field correlations. Carefully choosing the length scales of the disorder in the sample allows us to investigate and discriminate between transverse and longitudinal coherence properties. The longitudinal coherence properties of the x-ray beam permits us, for example, to estimate the duration of the x-ray pulses. This parameter is difficult to measure but crucial for experiments such as ultrafast magnetization dynamics where electronic and spin processes take place on time scales of 100 fs and below.

We present measurements of single shot speckle patterns at the LCLS in two different experimental geometries. The first one was performed in a small angle scattering (SAXS) geometry. The small scattering angle ensures that the longitudinal path length difference is negligible and that only the transverse coherence lengths are relevant. In contrast, the second measurement was performed at wide angles (WAXS) on a gold nanopowder. In this geometry, the maximum path length difference of the x-ray photons is of the order of the longitudinal coherence length, thus affecting the speckle contrast.

The LCLS linac was operated at a final electron energy of 14.2 GeV, electron bunch charge of 250 pC, and electron

pulse lengths of (100 ± 14) fs. X-ray pulses of photon energy of 8.96 keV, pulse energies of 1–2 mJ with a bandwidth $\Delta E/E \approx 10^{-3}$ were generated in the undulator. The experiment was performed at the x-ray pump-probe (XPP) instrument utilizing a Si(111) channel cut monochromator with a bandwidth of $\Delta E/E = 1.36 \times 10^{-4}$. The beam was focused by beryllium compound refractive lenses to a size of 9 (h) $\times$ 3 (v) μm^2 at the sample position (see Fig. 1).

Concentrated suspensions (52 vol %) of hard sphere colloidal particles (PMMA in decalin) of diameter 100 nm were filled in quartz capillaries of diameter 0.7 mm. The parasitic scattering from upstream optical components is reduced by placing a 100 μm pinhole in front of the sample. The detector (Princeton LCX CCD, 20 μm pixel size) was placed 4.36 m downstream from the sample. The transmitted beam was blocked by a tungsten beamstop of 3.5 mm diameter. The energy density deposited on the sample is of the order of 4×10^5 mJ/cm^2 per shot. It destroys the sample as evidenced by video microscopy. However, the recorded SAXS patterns are identical to those measured at storage ring sources confirming that the pulse duration is short enough for the signal not being compromised by the disintegration process. A fresh part of the sample is illuminated for each new pulse by translating the sample holder. We thus collected series of single shot speckle patterns from the sample. The SASE fluctuations lead to a significant x-ray intensity fluctuation downstream of the monochromator.

Figure 1 (upper right) shows a typical single shot speckle pattern of a colloidal suspension (Q range covered by the CCD camera is $Q_{\max} = 0.15$ nm^{-1}). A pronounced grainy (speckle) structure of the diffraction pattern is observed

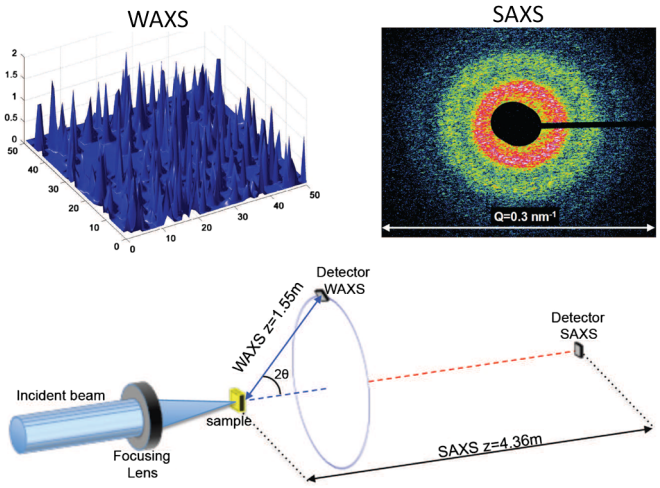

FIG. 1 (color online). Schematics of the single pulse LCLS coherent diffraction experiment of an Au nanopowder at the Au(111) diffraction peak $Q = 26$ nm^{-1} (WAXS, upper left) and of a colloidal solution in SAXS geometry (upper right). Both experiments have been performed with a photon wavelength of $\lambda = 1.37$ Å.

which reflects the exact spatial arrangement of the particles during the exposure time. The angular size of the speckles is given by λ/L, where L denotes the beam size and λ the photon wavelength. The shape anisotropy of the individual speckles is due to the different beam sizes in the vertical and horizontal direction [speckle sizes 15 μrad (h) and 44 μrad (v)]. The SAXS pattern shows the typical concentric rings of the form factor of the spherical colloidal particles. The intense red ring close to the beamstop is the peak of the static structure factor representing the spatial correlations of the particles in the solution.

The most direct quantity that can be deduced from a speckle pattern is the contrast which is closely related to the coherence properties of the beam. We define here the contrast as the normalized variance of the intensity fluctuations in a region with spatially uniform mean intensity, $\beta = \sqrt{\mathrm{Var}(I)}/\langle I \rangle$. The contrast is connected to the coherence properties of the beam via $\beta = 1/\sqrt{M}$, where M is the number of modes or $\beta = |\gamma(R = 0)|$, where γ is the mutual coherence function of the fields at separation R [18].

For deducing the contrast we analyzed rings of constant $|Q|$ (mean intensity $\langle I \rangle \approx 2$ photons per pixel per shot) in the speckle patterns and computed the variance from the intensity fluctuations. Figure 2 (top) displays the contrast as a function of shot number at $Q = 6 \times 10^{-2}$ nm^{-1}. The contrast is fluctuating very closely to unity with an average contrast of $\langle \beta \rangle = 0.94 \pm 0.03$ indicating an almost fully transverse coherent beam in the focal area. This is in good agreement with simulations [19]. The shot-to-shot fluctuations of the contrast are small with the lowest measured contrast value of 0.85.

Another useful means of characterizing a speckle pattern is the intensity probability distribution function $p(I)$ given by [18]

$$p(I) = \frac{\Gamma(I + M)}{\Gamma(M)\Gamma(I + 1)} \left(1 + \frac{M}{\langle I \rangle}\right)^{-I} \left(1 + \frac{\langle I \rangle}{M}\right)^{-M}, \qquad (1)$$

where I is the number of photons, $\langle I \rangle$ the average photon number, and M is the number of modes. Figure 2 (middle) shows the histogram of a single shot speckle pattern together with two lines calculated via expression Eq. (1) for $M = 1$ (solid line) and $M = 2$ (dashed line), respectively. The data are very well described with a single mode ($M = 1$), while $M = 2$ already deviates strongly from the data.

The spatial intensity correlation function $g(R) = \langle I(r + R)I(r) \rangle / \langle I(r) \rangle^2 = |\gamma(R)|^2 + 1$ yields information about the mutual coherence function $\gamma(R)$. We calculated the spatial intensity correlation functions in both vertical and horizontal direction. Both $\gamma(R)$ functions can be described by an exponential $\gamma_{v,h}(R) = \exp(-R/R_{v,h})$ [as displayed for the horizontal direction in Fig. 2 (bottom)]. Assuming that the illuminating beam profile is of Lorentzian shape we can connect the speckle size $R_{v,h}$ with the beam size (FWHM

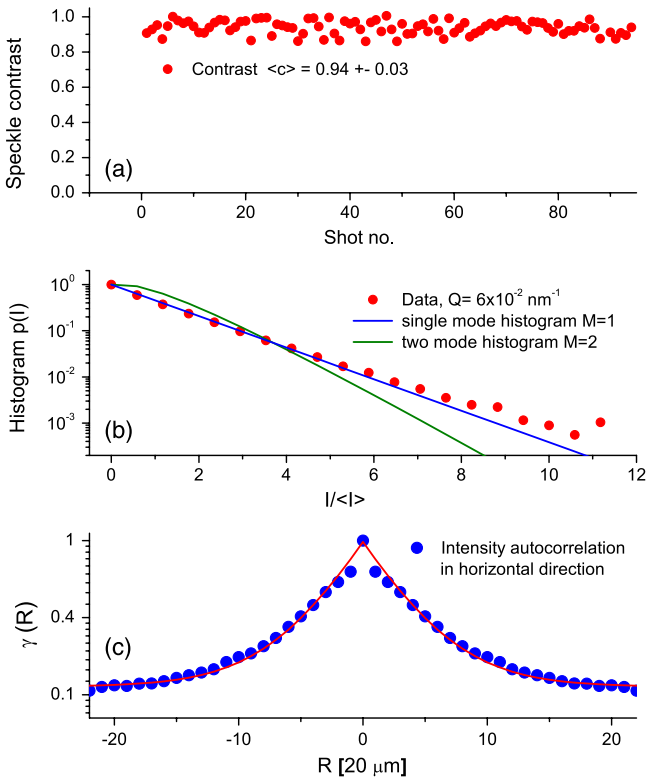

FIG. 2 (color online). (a) Single pulse speckle contrast (visibility) for a series of shots from the LCLS recorded in SAXS setup ($Q = 6 \times 10^{-2}$ nm^{-1}). (b) Histogram of the intensity distribution from a typical single pulse speckle pattern. Blue solid line: fit according to Eq. (1) assuming a single transverse mode (fully coherent). The green line displays Eq. (1) assuming two transverse modes present for comparison. (c) Spatial intensity autocorrelation function in the horizontal direction yielding the speckle width and illumination function (R is the pixel coordinate on the camera).

σ) via $R_{v,h} = \lambda z/(2\pi\sigma_{v,h})$, where z is the sample-detector distance. We obtain values for the beam sizes of 3.3 and 9 μm in the vertical and horizontal direction, respectively, which is in very good agreement with the measured beam widths.

For the WAXS experiment a Au-nanopowder sample was used. The sample was produced by spreading a solution of Au and polyvinylpyrrolidone (PVP) on a thin kapton support. The thickness of the Au-nanopowder sample is (2.24 ± 0.36) μm. The detector was placed at a distance of 1.55 m from the sample at a vertical scattering angle $2\theta = 34°$ ($Q = 26$ nm^{-1}) to match the position of the Au(111) reflection (Fig. 1). The x-ray beam and free-electron laser parameters were the same as for the SAXS experiment. The energy density in the focused beam is large enough to destroy locally the sample as evidenced by a light flash from the sample. Series of single shot images were taken by moving the sample transversely to the beam.

The inset in Fig. 1 (upper left) shows a small portion of a single shot speckle pattern from the Au sample. Here the speckle pattern is reflecting the spatial arrangement of the Au atoms on a length scale of 0.242 nm. The speckle pattern basically consists of 0, 1, 2, and 3 photon events. On average we observed 2.5×10^{-2} photons per pixel per single shot. Comparing the intensities with the SAXS case we find that single shot scattering intensities at large Q value are low and statistics can only be gained by a large number of pixels.

By histogramming the intensity one can deduce the speckle contrast as shown previously. We evaluated the speckle contrast for 62 single shot speckle patterns [see Fig. 3 (top)]. A considerable shot-to-shot fluctuation of the speckle contrast with values varying between 0.1 and 0.47 is observed with a standard deviation $\sigma = 0.08$. The average contrast is $\langle\beta\rangle = 0.26 \pm 0.02$.

At large scattering angles the path length difference of the x rays scattered at different positions in the sample becomes comparable to the longitudinal coherence length $\xi_l = \tau_c c$ [20], with τ_c denoting the coherence time and c the speed of light. Thus the speckle contrast is reduced and its value depends on the spectral properties of the LCLS. Having established previously that the beam is transverse

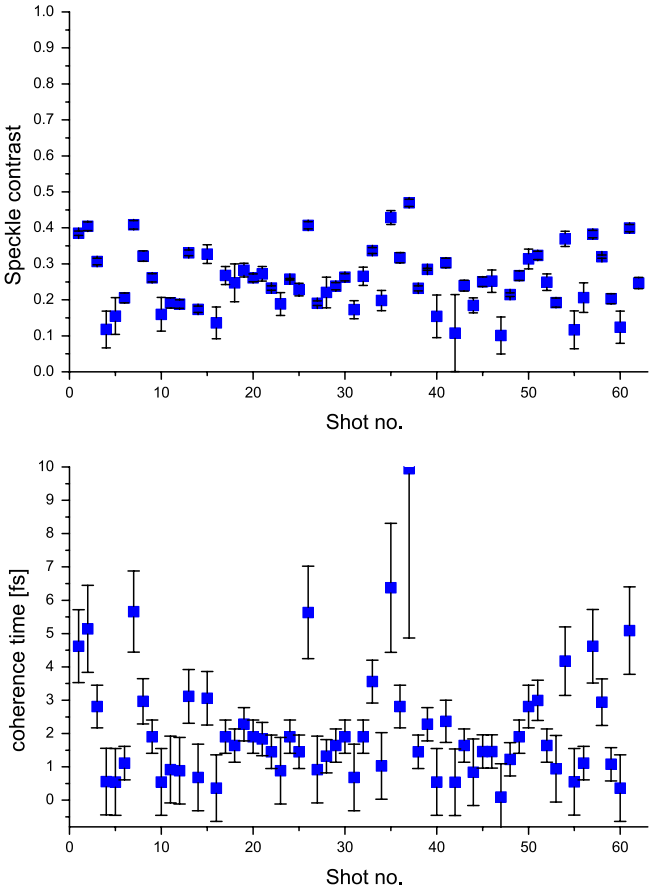

FIG. 3 (color online). Top: Series of single pulse speckle contrast measurements at $Q = 26$ nm^{-1}. Bottom: Shot-to-shot variation of the coherence time of the LCLS at 9 keV photon energy as deduced from the speckle contrast and Eq. (2).

fully coherent, we can calculate the speckle contrast as (assuming a Gaussian spectrum)

$$\beta^2 = \frac{2}{L^2W^2}\int_0^L dx(L-x)\int_0^W dy(W-y) \times \{\exp[-\pi(Ax+By)^2] + \exp[-\pi(Ax-By)^2]\}, \quad (2)$$

with L denoting the beam size and W the sample thickness [20–22]. A and B depend on the coherence time τ_c, $k_0 = 2\pi/\lambda$, and Q, and are given by $A = Q/(\tau_c k_0 c) \times \sqrt{1-(Q/2k_0)^2}$ and $B = Q^2/(2\tau_c k_0^2 c)$, respectively. In order to compare the model with our data, we take an additional smearing effect caused by the detector resolution into account. Using the mean contrast $\langle\beta\rangle = 0.26$ as input, a numerical inversion of Eq. (2) yields a mean coherence time of $\langle\tau_c\rangle = (2 \pm 1)$ fs. This value is in good agreement with results from simulations yielding $\tau_c \simeq 2.5$ (FWHM) [23]. The measured τ_c corresponds to a Gaussian energy bandwidth (FWHM) of $(\Delta E/E)_G = 0.66\lambda/(c\tau_c) = 1.5 \times 10^{-4}$, which is close to the bandwidth of 1.36×10^{-4} of the Si(111) monochromator.

The data also allow us to deduce the coherence time on a single shot basis [Fig. 3 (bottom)]. The error bars represent a confidence interval which takes a 10% fluctuation in beam size and the error of the measured contrast into account. Most of the data fall into a region of coherence times from 0.5 to 2.5 fs while we also observed some shots providing a larger coherence time in the region around 4–6 fs. The mean coherence time deduced from the single shot data set is $\langle\tau_c\rangle = 2.2$ fs (standard deviation 1.8 fs).

The theory of the SASE process yields an expression for the intensity probability distribution [10]

$$p(I) = \frac{\langle M_t\rangle^{\langle M_t\rangle}}{\Gamma(\langle M_t\rangle)}\left(\frac{I}{\langle I\rangle}\right)^{\langle M_t\rangle - 1}\frac{1}{\langle I\rangle}\exp\left(-\langle M_t\rangle\frac{I}{\langle I\rangle}\right), \quad (3)$$

where $\langle M_t\rangle$ is the average number of temporal modes and $\langle I\rangle$ the average intensity. By analyzing the data of the intensity monitor downstream of the monochromator, we can deduce the average number of temporal modes (Fig. 4). Fitting Eq. (3) to the data yields $M_t = 14.5 \pm 1$ temporal modes, which is in good agreement with $M_t = 16$ modes obtained from simulations. The number of modes allows us to estimate the average x-ray pulse duration (FWHM) behind the monochromator via $\langle T\rangle = M_t\tau_c = (29 \pm 14)$ fs. Thus the x-ray pulses seem considerably shorter than the electron bunch duration of 100 fs. This finding is consistent with simulations [23] and recent experiments [24,25], and will have major impact on a whole class of LCLS experiments that depend on a detailed knowledge of the pulse duration.

In summary, our experiments characterize and quantify the high coherence properties of the hard x-ray LCLS beam. The focused beam is transversely fully coherent with a mode number close to 1, while the average number of longitudinal modes is about 14.5. We demonstrated the possibility to measure single shot speckle patterns on atomic length scales. The mean coherence time downstream of the Si(111) monochromator is $2(\pm 1)$ fs. This implies an x-ray pulse duration of 29 ± 14 fs for 100 fs electron bunches.

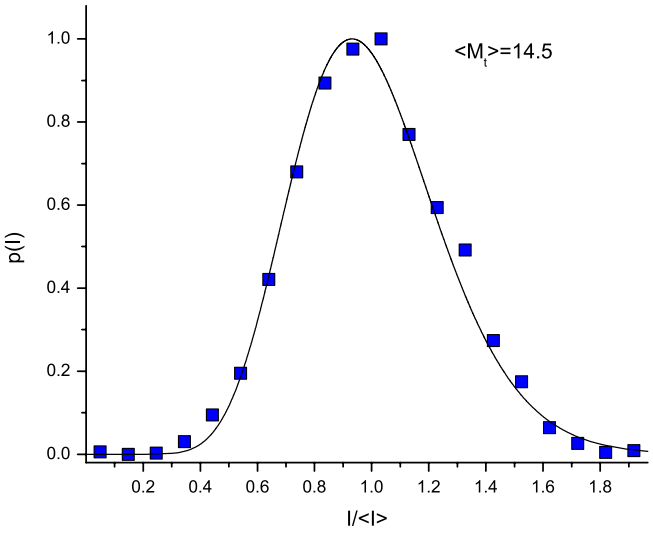

FIG. 4 (color online). Intensity probability density function of the intensity of the LCLS at 9 keV photon energy behind the Si(111) monochromator. The solid line represents the distribution [Eq. (3)] with $\langle M_t\rangle = 14.5$ temporal modes.

Portions of this research were carried out at the Linac Coherent Light Source (LCLS) at the SLAC National Accelerator Laboratory. LCLS is an Office of Science User Facility operated for the U.S. Department of Energy Office of Science by Stanford University. P. H. F. and G. B. S. were supported by the U.S. Department of Energy, Office of Basic Energy Sciences, Division of Materials Sciences and Engineering. The Au nanopowder samples were supplied by A. Plech. P. W., M. C.-C., and S. B. thank M. Rühle for his encouraging support.

*christian.gutt@desy.de

[1] P. Emma *et al.*, Nature Photon. **4**, 641 (2010).
[2] H. N. Chapman *et al.*, Nature (London) **470**, 73 (2011).
[3] M. M. Seibert *et al.*, Nature (London) **470**, 78 (2011).
[4] G. B. Stephenson, A. Robert, and G. Grübel, Nature Mater. **8**, 702 (2009).
[5] P. Wochner, C. Gutt, T. Autenrieth, T. Demmer, V. Bugaev, A. Diaz-Ortiz, A. Duri, F. Zontone, G. Grübel, and H. Dosch, Proc. Natl. Acad. Sci. U.S.A. **106**, 11 511 (2009).
[6] G. Grübel, G. B. Stephenson, C. Gutt, H. Sinn, and T. Tschentscher, Nucl. Instrum. Methods Phys. Res., Sect. B **262**, 357 (2007).
[7] S. Eisebitt, J. Lüning, W. F. Schlotter, M. Lörgen, O. Hellwig, W. Eberhardt, and J. Stöhr, Nature (London) **432**, 885 (2004).
[8] C. Gutt *et al.*, Phys. Rev. B **81**, 100401(R) (2010).

[9] E. L. Saldin, E. A. Schneidmiller, and M. V. Yurkov, *The Physics of Free Electron Lasers* (Springer-Verlag, Berlin, 2000).
[10] E. L. Saldin, E. A. Schneidmiller, and M. V. Yurkov, Opt. Commun. **148**, 383 (1998); Eq. (3) is expected to be valid at least in the linear regime.
[11] E. L. Saldin, E. A. Schneidmiller, and M. V. Yurkov, Opt. Commun. **281**, 1179 (2008).
[12] Z. Huang and K. J. Kim, Phys. Rev. ST Accel. Beams **10**, 034801 (2007).
[13] M. V. Yurkov, Nucl. Instrum. Methods Phys. Res., Sect. A **483**, 51 (2002).
[14] R. Mitzner, B. Siemer, M. Neeb, T. Noll, F. Siewert, S. Roling, M. Rutkowski, A. A. Sorokin, M. Richter, P. Juranic, K. Tiedtke, J. Feldhaus, W. Eberhardt, and H. Zacharias, Opt. Express **16**, 19 909 (2008).
[15] A. Singer, I. A. Vartanyants, M. Kuhlmann, S. Duesterer, R. Treusch, and J. Feldhaus, Phys. Rev. Lett. **101**, 254801 (2008).
[16] S. Roling *et al.*, Phys. Rev. ST Accel. Beams **14**, 080701 (2011).
[17] I. A. Vartanyants *et al.*, Phys. Rev. Lett. **107**, 144801 (2011).
[18] J. W. Goodman, *Speckle Phenomena in Optics* (Roberts and Company, Greenwood Village, CO, 2007).
[19] Y. Ding, Z. Huang, and S. A. Ocko, Report No. SLAC-PUB-14235, 2010.
[20] D. L. Abernathy, G. Grübel, S. Brauer, I. McNulty, G. B. Stephenson, S. G. J. Mochrie, A. R. Sandy, N. Mulder, and M. Sutton, J. Synchrotron Radiat. **5**, 37 (1998).
[21] A. R. Sandy, L. B. Lurio, S. G. J. Mochrie, A. Malik, G. B. Stephenson, J. F. Pelletier, and M. Sutton, J. Synchrotron Radiat. **6**, 1174 (1999).
[22] M. Sutton (private communication).
[23] E. M. Schneidmiller and M. Yurkov (private communication); see also DESY Report No. 11-152, 2011.
[24] L. Young *et al.*, Nature (London) **466**, 56 (2010).
[25] S. Düsterer *et al.*, New J. Phys. **13**, 093024 (2011).